P1.8 MICROPHYSICAL PROPERTIES OF ARCTIC MIXED-PHASE CLOUDS USING GROUND-BASED REMOTE SENSORS

Jennifer M. Comstock*, Connor J. Flynn, Charles N. Long, Roger T. Marchand, James H. Mather, Sally A. McFarlane, Albert Mendoza, David D. Turner, and Kevin Widener

Pacific Northwest National Laboratory, Richland, Washington

1. INTRODUCTION

Arctic clouds are characterized as being stratiform and optically thin, and on average ~50% are mixed-phase clouds that occur during all seasons (Intrieri et al. 2002). Arctic mixed-phase clouds have been observed to persist for days, even though the clouds are precipitating ice. Mixed-phase cloud processes are poorly understood and thus the mechanisms that allow for the maintenance of these clouds are uncertain. Numerical modeling studies suggest that incorporation of ice and mixed-phase in models influences the cloud evolution, cloud-scale dynamics and the surface energy budget (Harrington and Olsson, 2001). Determining the microphysical properties and phase is a crucial link in understanding the dynamical and radiative processes of Arctic mixed-phase clouds.

In this paper, we will present preliminary results of combined radar-lidar retrievals of microphysical properties for Arctic mixed-phase clouds. We also present results from a spectral infrared retrieval of cloud properties. These cloud properties can be used by the modeling community to help understand how small-scale inhomogeneities contribute to the maintenance of Arctic mixed-phase clouds and for development of improved parameterizations for global circulation and cloud resolving models.

2. INSTRUMENTS AND DATA

During the Department of Energy Atmospheric Radiation Measurement (ARM) program's Mixed-Phase Arctic Cloud Experiment (M-PACE; 27 September-22 October 2004), the PNNL (Pacific Northwest National Laboratory) Atmospheric Remote Sensing Laboratory (PARSL) deployed a variety of active and passive remote sensors at Oliktok Point, AK (70º 30' 5" N, 149º 51' 33" W). The instruments supplied for this deployment include high spatial resolution lidar, Doppler cloud radar, a dual-channel microwave radiometer (MWR), and the University of Wisconsin - Madison Atmospheric Emitted Radiance Interferometer (AERI). Various passive solar and infrared radiometers, balloon-borne radiosondes, and standard meteorological instruments were also deployed at Oliktok Point during M-PACE.

The primary instruments used in this study are the dual-polarization lidar, the 94 GHz radar, the MWR and AERI. During M-PACE, PARSL deployed a polarization diverse, 523 nm wavelength lidar that was designed and built at PNNL. This lidar system detects both the co-polarized and cross-polarized returned signals, which are used to determine the depolarization ratio δ. The lidar was operated with pulse energies of 100 μJ and a pulse rate of 2000 Hz. The temporal averaging is ~30 s and the spatial range resolution is ~30 m.

The 94 GHz radar was designed and built at PNNL and is based on the Lhermitte (1987) design, but improved by PNNL researchers to increase sensitivity. The radar has a transmit power of 1000 W, a maximum pulse repetition frequency of 20 kHz and an estimated sensitivity of -31 dBZ at 10 km. The data system is designed to record complete Doppler moments (reflectivity, velocity, and spectral width), power, spectra, and I/Q analog data.

The MWR is manufactured by Radiometrics Inc. and is a dual-frequency radiometer that operates at 23.8 and 31.4 GHz, which allows the simultaneous determination of column integrated water vapor and liquid water. The AERI measures the absolute infrared spectral radiance in the zenith direction with a 1.3° field-of-view. The spectral range is 400-3300 cm^{-1} wavenumber (or 25-3 μm wavelength) and has a spectral resolution of 1 cm^{-1}. During M-PACE, the AERI was operated in "rapid sample" mode, which allows for approximately 30-s temporal resolution. In this study, we combine these instruments, along with standard radiosonde thermodynamic profiles, to retrieve cloud phase and microphysical properties in Arctic clouds observed during M-PACE.

3. DETERMINATION OF CLOUD PHASE

We have developed a simple composite cloud and aerosol mask using a combination of radar and lidar data (Fig. 1). To distinguish cloud phase, we use simple thresholds determined by the lidar backscatter and depolarization ratio. In regions where only the radar detects cloud, the phase is indeterminate at this stage in our analysis. Techniques exist for determining cloud phase directly from radar Doppler spectra (Shupe et al. 2004); however we have not yet implemented this algorithm for this preliminary analysis.

* *Corresponding author address:* Jennifer M. Comstock, Pacific Northwest National Laboratory, Richland, WA 99352; email: jennifer.comstock@pnl.gov.

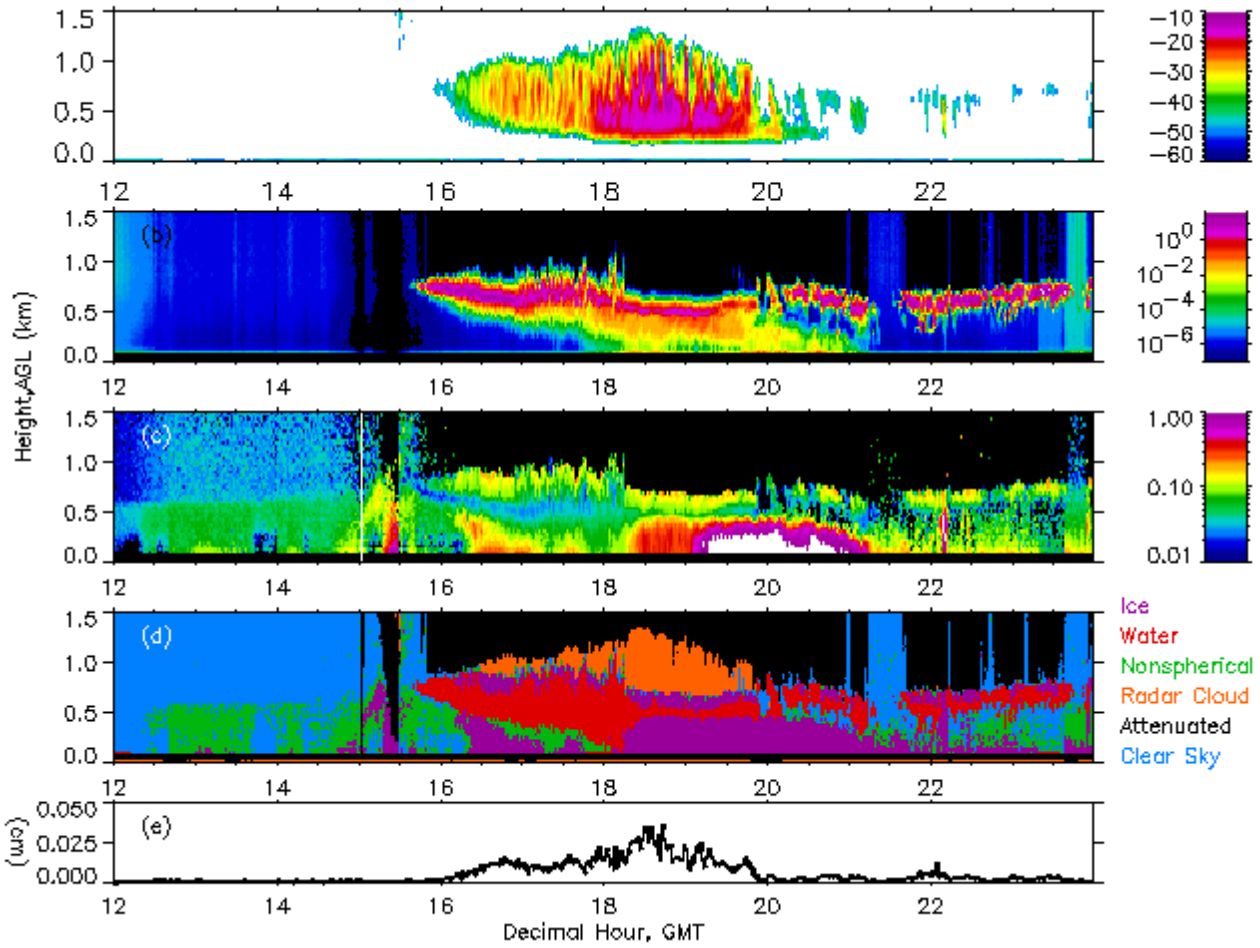

Figure 1. Time vs. height display of radar reflectivity in dBZ (a), lidar copolarized backscatter in relative units (b), lidar depolarization ratio (c), aerosol and cloud mask (d), and MWR column liquid water in cm (e). This case was observed on 28 September 2004 by the PARSL remote sensing instruments located at Oliktok Point during M-PACE.

The cloud observed on 28 September 2004 is a mixed-phase cloud with an extensive water layer. Ice appears to be falling from the water layer and ice and possibly snow precipitation occurs between 1830 and 2100 UTC. It is not uncommon for ice precipitation to fall from Arctic mixed-phase clouds (Intrieri et al. 2002). The co-located MWR (Fig. 1e) also detects water during this same time period, with smaller amounts occurring after ~2000 UTC, when most of the heavier precipitation has passed. The lidar depolarization data also reveals an aerosol layer below 600 m prior to the passing of the cloud layer (1200 – 1530 UTC). It appears that this aerosol or haze layer is interacting with the mixed-phase cloud and continues to persist (but to a lesser extent) after the cloud system has passed (2330 UTC).

The black region in Fig. 1d indicates times when the lidar beam is attenuation limited and no signal is returned to the lidar. This usually occurs when the visible optical depth exceeds ~3. The orange regions indicate points when the radar detects cloud, but the lidar does not. Just prior to 1530 UTC, the lidar becomes attenuated, but still indicates some depolarized signal. There is likely some precipitation occurring at this time. The depolarization ratio is slightly enhanced in some regions between 0.5 and 1.0 km, which may indicate the presence of ice. Due to the presence of large amounts of column liquid water (Fig. 1e) we believe that this cloud is primarily composed of water with ice precipitating below the cloud base. The increase in lidar depolarization ratio at ~0.75 km might be a result of multiple scattering of the lidar beam. More analysis of radar spectra and *in situ* data is required to verify this result.

4. MICROPHYSICAL RETRIEVALS

4.1 *Lidar-radar retrieval*

We retrieve vertical profiles of cloud particle effective radius and mass using the combined lidar-radar

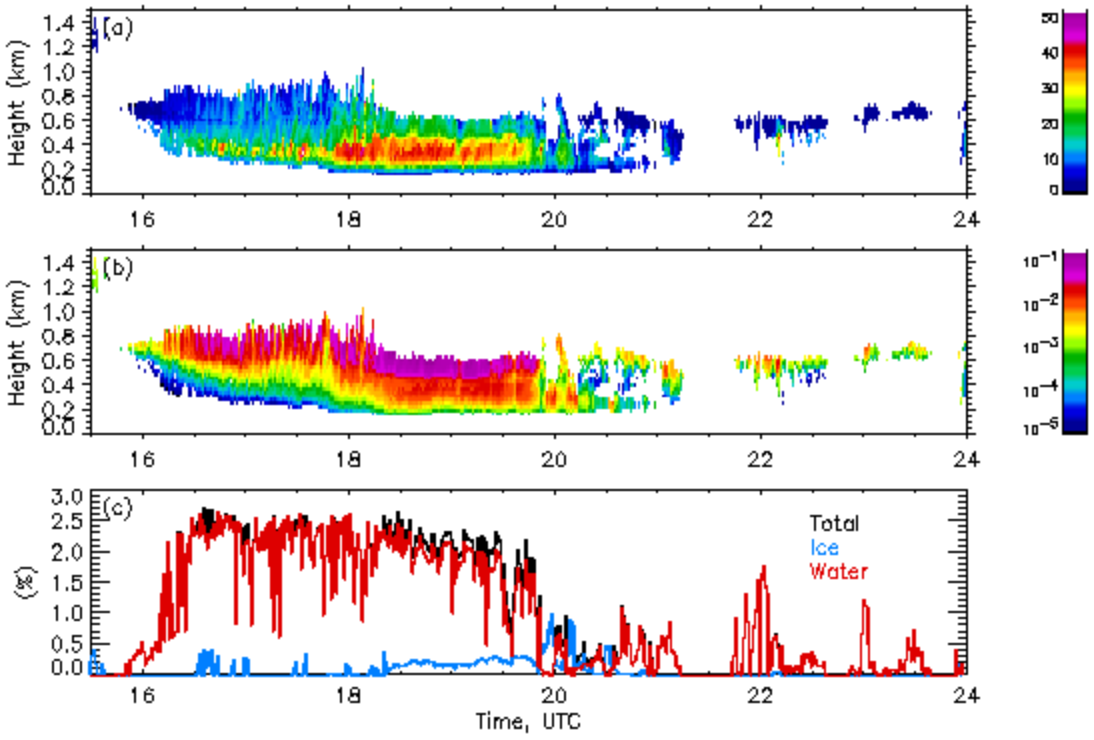

Figure 2. Lidar-radar retrieval of effective radius in μm (a), mass content in g m^{-3} (b), and visible optical depth (c) observed on 28 September 2004. The ice, water, and mixed-phase results for r_e and mass content are combined on each figure. The lidar-radar retrieval is performed only during times when both lidar and radar detect cloud. Refer to Fig. 1 for details of cloud phase and boundaries.

algorithm of Donovan and van Lammeren (2001). The basic principles of the algorithm are to utilize the ratio of the measured radar reflectivity (*Z*) to the lidar extinction (α), *Z*/α, and relate this ratio to a characteristic particle size (R′) to retrieve particle effective radius and cloud mass content for both ice and water. For example, the parameter R′ for water drops is

$$R' = \left(\frac{\langle r^6 \rangle}{\langle r^2 \rangle} \right)^{1/4} \qquad (1)$$

where r is the particle radius and the angle brackets denote an average over the size distribution. This equation is constructed based on the theory that at lidar and radar wavelengths the total scattering is proportional to $\langle r^2 \rangle$ and $\langle r^6 \rangle$, respectively. R′ and the ratio Z/α are related using regression analysis. Here we assume a gamma distribution of hexagonal columns to relate R′ to the effective radius r_e. The hexagonal columns are defined according to the scattering properties of Yang et al. (2000). This algorithm treats cloud identified as ice and water separately and also treats mixed-phase clouds by assuming the measured volume contains some fraction of ice and water. The R′ vs. Z/α relationships and particle density are adjusted by interpolation.

In these preliminary results, we use the cloud mask (Fig. 1d) to identify water and ice regions in the cloud. We perform the retrieval on the cloud portions only, excluding the ice precipitation regions from the calculations. The retrieval is performed only on regions when both the radar and lidar detect cloud.

Retrievals of water/ice/mixed-phase effective radius (Fig. 2a) indicate that the upper/middle portions of the cloud are dominated by small particles (in this case primarily water droplets). The lower portions of the cloud are composed of large particles that are likely dominated by large ice crystals. The smallest particle sizes are found in the regions containing water. Keep in mind that the cloud top in Fig. 2 is not necessarily the actual cloud top, but only the top of the retrieved cloud properties (refer to Fig. 1 for actual cloud boundaries). The mass content is highest at the top of the retrieved cloud properties (Fig. 2b), which indicates that the water regions with small particles contributes to the majority of the cloud mass. This is also apparent in the optical depth (Fig. 2c) where water is the primary contributor to the total optical depth.

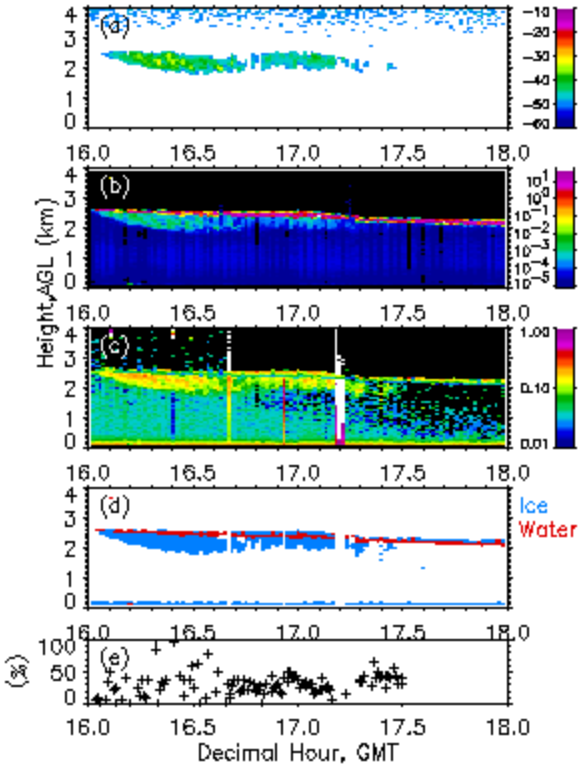

Figure 3. Example of mixed-phase cloud observed on 15 October 2004 at Oliktok Point. The 5 panels include radar reflectivity in dBZ (a), lidar copolarized backscatter in relative units (b), lidar depolarization ratio (c), cloud mask (d), and ice fraction in % retrieved using MIXCRA. The lidar and radar data are averaged for 1 min temporally and 30 m vertically.

4.2 *AERI mixed-phase retrieval*

Turner (2003, 2004) has developed a mixed-phase cloud microphysical property retrieval algorithm (MIXCRA) which retrieves cloud optical depth, ice fraction (phase), and the particle sizes of the liquid and ice particles in single layer clouds from AERI radiance observations. The technique takes advantage of the stronger absorption coefficient of ice, relative to water, in the 800 - 1000 cm^{-1} spectral region, whereas the absorption of liquid water is stronger than ice absorption from 350 - 600 cm^{-1}. This technique is limited to clouds with optical depths less than approximately 6; clouds with larger optical depths are virtually opaque in the thermal infrared. MIXCRA's ability to retrieve cloud phase is limited to conditions where the precipitable water vapor (PWV) is less than 1 cm, for when the PWV is larger than 1 cm, the strong water vapor absorption in the rotational water band make the 350 - 600 cm^{-1} spectral region opaque. However, in the Arctic, many boundary layer clouds have optical depths less than 6 and the PWV is often less than 1 cm in the fall, winter, and spring, making MIXCRA an excellent tool to retrieve cloud microphysical properties.

On 15 October 2004, a more typical Arctic mixed-phase was observed at Oliktok Point (Fig. 3). This cloud is composed of a thin water layer (identified by the low δ and strong lidar backscatter in Figs. 3b and 3c) with ice crystals falling below the water layer. The radar detected the ice portion of the cloud, but the water layer appears to be below the sensitivity of the radar, presumably due to the presence small water droplets in the water layer. At ~1730 UTC, the ice sedimentation ceases leaving just the water layer. The MWR column liquid water measurement (not shown) was below the instrument uncertainty level (<20 g/m^2). The MIXCRA retrieval indicates that this low liquid water path cloud consists of ~10 to 50% ice (Fig. 3e).

During this same time period, the lidar-radar algorithm retrieved both water and ice effective radius and mass content (Fig. 4). During the first 45 min (1600-1645 UTC), the ice layer was characterized by stronger backscatter (Fig. 3b) and larger radar reflectivity (Fig. 3a) than later in the observation period (after 1645 UTC). These stronger signals correspond with larger ice mass. After ~1645 UTC, the thin water layer is composed of very small water droplets, which correspond to large water contents. Note that since the radar did not detect the water layer before 1645, but did later in the time period, the water layer after 1645 may actually consist of both water and ice. The radar is typically not sensitive to very small water droplets, but will detect any ice in the layer.

5. SUMMARY AND OUTLOOK

Here we have presented preliminary results for a few cases during the recent ARM M-PACE field experiment that focused on Arctic mixed-phase clouds over the North Slope of Alaska. We have developed a simple mask to identify cloud phase by combining lidar backscatter and depolarization, as well as radar reflectivity measurements. We have also applied the combined remote sensor algorithm of Donovan and van Lammeren (2001) to retrieve particle effective radius and mass content. These results are just a first look at the multitude of data accumulated during this experiment.

In the future, we will improve the cloud mask by incorporating radar power spectra for identification of cloud volumes that contain both ice and water, as well as analyze *in situ* data for verification of our results. We would also like to improve the treatment of mixed-phase clouds in the microphysical retrievals. By learning more about the particle size distributions and contributions of ice and water in mixed-phase clouds through analysis of aircraft measurements during M-PACE, we can refine the treatment of these clouds in the retrieval algorithm. Since the AERI is sensitive to cloud phase (Turner 2003), we can also incorporate AERI spectral measurements to constrain the total water and ice contents in the cloud and further quantify the contribution of small ice crystals. Ultimately, with the further refinement of these algorithms these data will

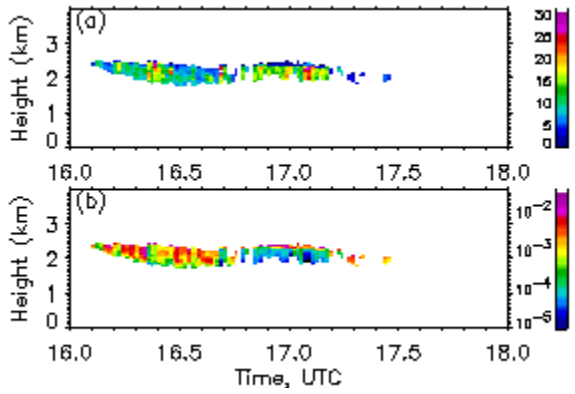

Figure 4. Lidar-radar retrieval of ice/water effective radius in μm (a) and cloud ice/water mass in g m^{-3} (b) observed on 15 October 2004.

provide a useful tool for better understanding Arctic mixed-phase cloud processes.

Acknowledgements. We would like to thank Dr. D. Donovan for making the lidar-radar retrieval available to us. This research was supported by the Climate Change Research Division of the U.S. Department of Energy as part of the Atmospheric Radiation Measurement (ARM) Program.

6. REFERENCES

Donovan, D. P., and A. C. A. P. van Lammeren, 2001: Cloud effective particle size and water content profile retrievals using combined lidar and radar observations - 1. Theory and examples. *J. Geophys. Res.,* **106**, 27425-27448.

Harrington, J. Y., and P. Q. Olsson, 2001a: Parameterization of cloud optical properties for use in bulk and bin microphysical models. Implications for the Arctic cloudy boundary layer. *Atmos. Res*. **57**, 51-80.

Lhermitte, R.M., 1987. "A 94-GHz doppler radar for cloud observations." *J. Atmos. Ocean. Tech.,* **4**, 36-48.

Intrieri, J. M., M. D. Shupe, T. Uttal, and B. J. McCarty, 2002: An annual cycle of Arctic cloud characteristics observed by radar and lidar at SHEBA. *J.Geophys. Res.,* **107**, 10.1029/2000JC000423.

Shupe, M.D., P. Kollias, S. Y. Matrosov, and T. L. Schneider, 2004: Deriving mixed-phase cloud properties from Doppler radar spectra, *J. Atmos. and Ocean. Tech.,* **21**, 660-670.

Turner, D.D., 2003: Microphysical properties of single and mixed-phase Arctic clouds derived from ground-based AERI observations. Ph.D. dissertation, University of Wisconsin-Madison, Madison, WI, 167 pp. Available from http://www.ssec.wisc.edu/library/turnerdissertation.pdf.

Turner, D.D., 2004: Arctic mixed-phase cloud properties from AERI-lidar observations: Algorithm and results from SHEBA. *J. Appl. Meteor*, in press.

Yang, P., K.N. Liou, K. Wyser, and D. Mitchell, 2000: Parameterization of the scattering and absorption properties of individual ice crystals. *J. Geophys. Res.*, **105**, 4699-4718.